**Title**
Adaptive Cancellation of Parasitic Coupling



**Journal**
Journal of Microelectromechanical Systems, 27(5)

**ISSN**
1057-7157

**Authors**
Ge, Howard H
Behbahani, Amir H
Gibson, James Steve
et al.

**Publication Date**
2018-10-01

**DOI**
10.1109/jmems.2018.2855103

Peer reviewed

# Adaptive cancellation of parasitic coupling

Howard H. Ge, Amir H. Behbahani, James S. Gibson, and Robert T. M'Closkey†
Mechanical and Aerospace Engineering
Samueli School of Engineering and Applied Science
University of California, Los Angeles, CA 90095

***Abstract*—This paper reports a signal processing technique that adaptively identifies a finite-impulse-response (FIR) model of the parasitic coupling between the input ports and the output ports of a microelectromechanical resonator. The identified model is used as a feedforward filter to reduce the severity of the parasitic coupling by subtracting the filtered input port signal from the resonator's output port signal. The compensated signals reveal the resonator's motional response, which was previously obscured by the coupling, so that modal frequency and quality factor measurements can be performed. The experimental results also show that the adaptive filter tracks changes in the parasitic coupling during turn-on and warm-up periods. More than 30dB of suppression of the parasitic coupling is achieved over a broad frequency band. The adaptive FIR filter is implemented on the signal processing equipment that is used to gather resonator stimulus-response data so no modifications to the resonator or its buffer electronics are required.**

***Index Terms*—Microelectromechanical devices, Resonators, Adaptive filters, Parasitics**

## I. Introduction

Microelectromechanical (MEM) devices typically possess high surface-to-volume ratios and have relatively thinly layered construction. Consequently, they are often subject to undesirable parasitic currents that couple input and output electrodes. The coupling can present a significant problem since its effects can often dominate the electrical measurements in capacitively transduced devices. Parasitic coupling in most instances is capacitive in nature and can be attributed to several sources: direct overlapping area of the transducer surfaces, coupling through the substrate, close proximity of inter-connnects, and inadvertent coupling through the external packaging [1, 2].

Many studies have been devoted to find ways to mitigate the parasitic feedthrough. A common and effective practice is to employ differential sensing and/or differential forcing schemes so that the parasitic coupling can be reduced by common mode rejection [2–4]. Techniques in which the device is parametrically driven with higher harmonics, and/or the sensing accomplished via a different modality, i.e. piezo-sensitive versus capacitive pickoffs, have also proved effective [5]. In [1], a tunable matching structure is deliberately introduced to mirror the feedthrough of the primary structure, thereby providing a subtraction reference. Most of these techniques rely on precise matching of geometrical features and electrical parameters, and often requires tuning of individual devices. Furthermore, even after careful tuning and matching, effective cancellation can only be achieved under the most ideal conditions as any deviation from the tuned operating point can drastically alter the coupling capacitance.

Other approaches to overcoming parasitic coupling rely on testing and signal processing techniques as opposed to modifying the device design. Two such techniques are proposed in [6]. The first is a time-domain gated excitation and detection approach in which the excitation and detection are performed over different, non-overlapping, time intervals. During the detection phase, the excitation signal is "off" which eliminates any excitation-to-pick-off coupling. The second technique, called electromechanical amplitude modulation (EAM), adds an AC dither voltage to the resonator's DC bias. Only the motional current is modulated by the AC dither, which produces sidebands about the dither frequency. Since the parasitic coupling current remains in the excitation frequency band, the dither signal and it's sidebands are separated in the frequency domain from the coupling-induced signal. Thus, the pick-off signal is filtered to remove the parasitic coupling components and then demodulated with the dither to shift the sidebands back to the correct frequency.

This study presents a nonintrusive method that is implemented in the downstream signal processing of the device signals, and can be employed either alone or as a supplement to any of the aforementioned techniques. The proposed method uses real-time adaptive identification of a parasitic coupling model that is used a feedforward filter to cancel the effects of the parasitic coupling to a significant degree. While the technique may not yet be amenable for integration into microdevices, it does provide a high degree of flexibility since the coupling transfer function is not constrained to a given passive circuit model.

The paper is organized as follows. Sec. II describes the test device and a model for the parasitic coupling, the latter which is used for expository purposes only and does not constrain the feedforward filter. This section also provides an example of a resonator with parasitic coupling that completely obscures the motional response. Sec. III discusses the identification of a (non-adaptive) finite impulse response filter for modeling the parasitic coupling. The non-adaptive filter is reformulated as an adaptive filter in Sec. IV and its ability to recover the motional frequency response is demonstrated. Sec. IV also provides evidence of the time-variant nature of the coupling (at least in the devices under test) and it is also shown that the feedforward technique does not bias or distort the frequency response estimates in devices with little to no parasitic coupling. Sec. V concludes the paper.

†Corresponding author, rtm@seas.ucla.edu.

## II. Problem motivation

### A. Description of test device

The compensation of parasitic coupling is developed in the context of the MEMS resonator illustrated in Fig. 1. The resonator consists of nested concentric rings of 20 $\mu$m width, which are connected to their neighbors by a system of staggered spokes. The diameter of the outermost ring is 10 mm. The outer ring is also surrounded by twenty four discrete electrodes with a 20 $\mu$m gap between the electrode face and ring sidewall. The electrodes can be configured for in-plane electrostatic actuation or capacitance sensing. The resonator is fabricated using a bonded wafer approach and has essentially three layers: the resonator-electrode layer, insulating oxide, and the die base. The resonator-electrode layer is 270 $\mu$m thick (111) Si and the base layer is 475 $\mu$m thick (100) Si. The base wafer is etched to create recessed gaps for clearance of the resonator rings and thermally oxidized for electrical isolation. A cross-section of the die illustrating the base wafer portion is shown in Fig. 2. The electrodes are co-etched with the resonator to maintain maximum alignment accuracy. This planar resonator was designed to function as a Coriolis vibratory gyroscope (CVG), eg. [7], and features multiple paired modes with natural frequencies near 6 kHz for the lowest frequency $n = 1$ pair, 13.5 kHz for the $n = 2$ pair and 24 kHz for the $n = 3$ pair. The integer $n$ refers to the dominant dependence of the mode shape on the angular coordinate $\theta$. In other words, the mode shapes for each pair modes can be approximately described by a weighted sum of $\cos(n\theta)$ and $\sin(n\theta)$ (these functions exactly describe the modes of a single uniform thin ring but are only approximate for more complicated ring-like structures like the one shown in Fig. 1). Furthermore, the anti-nodes of the paired modes subtend approximately $90/n^\circ$ so this impacts the placement of the forcing and pick-off electrodes if a given pair of modes is to be detected. Additional detail regarding the dynamics of this resonator are given in [8, 9], and CVG applications are reported in [10, 11]. Although the technique developed in this paper can be employed to identify any modes in MEM resonators, the present study is concerned with identifying the $n = 2$ pair of modes near 13.5 kHz in the presence of parasitic coupling.

Parasitic coupling between an excitation electrode ($E_3$ through $E_6$ –see the Fig. 1 caption) and a pick-off electrode ($E_1$ or $E_2$) can be interpreted using the circuit schematic in Fig 2. In order to minimize the number of wire bonds to the die a choice was made to tie the base silicon to the same bias source as the resonator (the resonator bias is denoted $V_B$). This is accomplished by opening the oxide on the base so that the wire bond pad which is used to connect the DC voltage bias to the resonator makes an ohmic contact with the base silicon. The connection between the resonator bias pad and the resonator itself is not shown in the cross-section. The wafer resistance is denoted $R_w$. Coupling is created because the bias source, which is typically either a battery operated reference or a programmable power supply, has non-zero source impedance. The source impedance is denoted $R_s$ in the circuit schematic. The electrode bond pads and electrodes

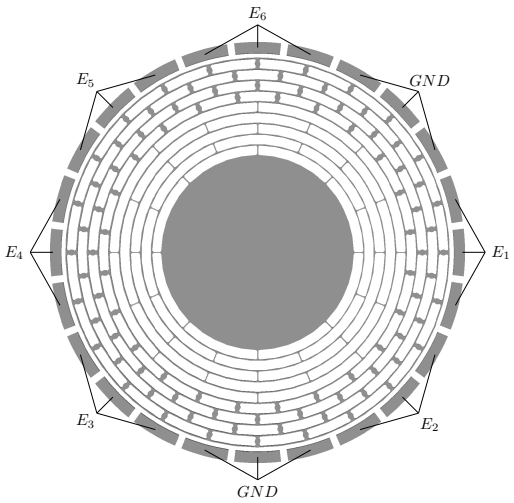


Fig. 1. Top view of the resonator with twenty four peripheral electrode segments. Individual electrode seqments are tied together to form a larger electrode. Electrodes $E_1$ and $E_2$ are used as pick-offs for measuring in-plane motion of the resonator. Electrodes $E_3$ through $E_6$ are used to electrostatically force the resonator. The electrodes labeled "$GND$" are grounded.

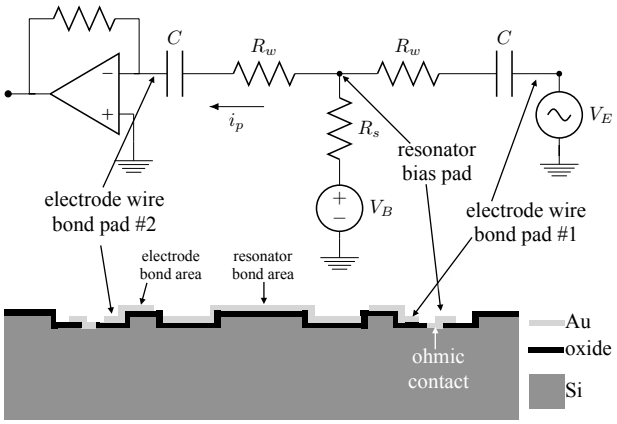


Fig. 2. Cross-section of base to which the resonator (not shown) is attached and a simple model for the parasitic current $i_p$ created by the electrode voltage $V_E$. The source impedance, die's base layer resistivity, bond pad-base capacitance, and resonator bias voltage are denoted $R_s$, $R_w$, $C$, and $V_B$, respectively.

themselves are capacitively coupled to the base silicon since they are separated by the insulating oxide. The capacitance is denoted $C$. The transfer function from the excitation electrode voltage ($V_E$ at "wire bond pad #1" in Fig. 2) to the parasitic current, $i_p$, appearing at the input to the trans-resistance buffer located at "wire bond pad #2" is given by,

$$i_p/V_E = \frac{Cs^2}{R_wC\left(2+\frac{R_w}{R_s}\right)s^2 + 2\left(1+\frac{R_w}{R_s}\right)s + \frac{1}{R_sC}}, \quad (1)$$

where $s$ denotes the Laplace transform variable. This transfer function has a high-pass characteristic with high-frequency magnitude approaching an asymptotic value of $R_s/(R_w^2 + 2R_sR_w)$. Thus, in general, if the source impedance is non-zero ($R_s \neq 0$), then the coupling current increases across all frequencies as the wafer resistivity decreases. Similar findings

relating the parasitic current to the base wafer resistivity were described in [6], albeit for a different device geometry.

The full instrumentation for excitation and detection of the resonator motion are illustrated in the block diagram in Fig. 3(a). As indicated in Fig. 2, the pick-off electrode currents are buffered by trans-resistance amplifiers, denoted by BUF in the Fig. 3 block diagram. A digital signal processor implements discrete-time filtering operations and interfaces to the sensor via analog-to-digital convertors (ADCs) and digital-to-analog convertors (DACs). The sample rate is 50 kHz. The total current produced at a pick-off electrode is the sum of the parasitic coupling current and the motional current induced by the time-rate-of-change of the capacitive gap between the electrode and resonator. The buffer outputs are filtered by anti-alias filters prior to sampling. The anti-alias filters are denoted as AAF in Fig. 3(a). The excitation electrodes are configured as differential pairs and the electrode arrangement in Fig. 1 optimally excites and senses the paired $n = 2$ modes. The differential excitation itself is useful in reducing parasitic coupling, however, even in this case the residual coupling is quite large in devices constructed with highly doped base wafers. Although (1) is useful for describing in general terms the source of the coupling, in practice, the parasitic coupling is more complicated and must also include the buffer and anti-alias filter dynamics.

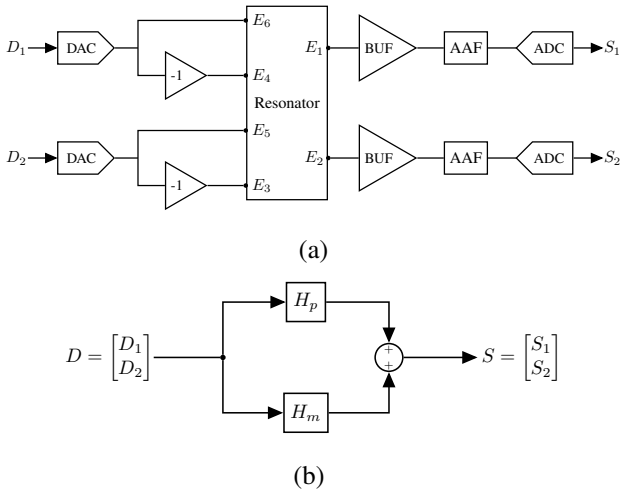


Fig. 3. (a) Block diagram showing the electrical interface to the resonator, and (b) representation as a motional subsystem, $H_m$, in parallel with the parasitic coupling, $H_p$.

## B. Example of parasitic coupling

The transfer function from input $D$ to output $S$ is denoted $S/D$ and has the form $S/D = H_p + H_m$, where $H_p$ is the transfer function of the parasitic coupling and $H_m$ is the transfer function associated with the motion of the resonator (Fig. 3(b)). An example of the frequency responses of a resonator with high parasitic coupling and a different resonator with low parasitic coupling is shown in Fig. 4. Specific channels of the frequency responses are denoted $S_q/D_p$ where the input is $D_p$, $p = 1, 2$, and the pick-off signal is $S_q$, $q = 1, 2$. The frequency responses are obtained using standard spectral estimation techniques (Welch's method [12]).

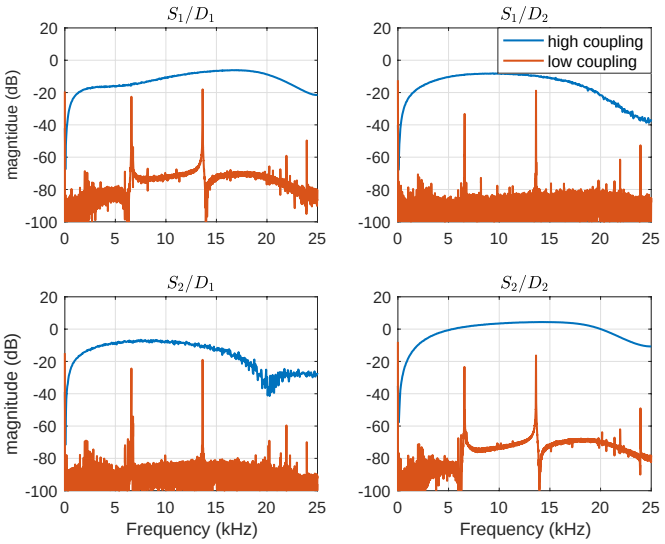


Fig. 4. Wideband frequency response of a resonator with high parasitic coupling and a resonator with low coupling. The modes in the high coupling case are masked by the coupling. The $n = \{1, 2, 3\}$ pairs are evident in the low coupling resonator near frequencies of $\{6, 14, 24\}$ kHz.

The resonator with high coupling was fabricated using a base wafer with 0.001-0.005 Ohm-cm resistivity, whereas the resonator with low coupling was fabricated using a base with 1-10 Ohm-cm resistivity. The roughly three to four order magnitude difference in resistivity is reflected in the same order of magnitude difference in the level of the parasitic coupling in Fig. 4. The same resonator bias source and buffer board was used for testing these die. The feedback resistor in the signal buffer is 10 MΩ (Fig. 2) which implies parasitic coupling currents on the order of 100 nA for the devices constructed with the 0.001-0.005 Ohm-cm resistivity base wafer. For devices constructed with the 1-10 Ohm-cm resistivity base wafers, the parasitic coupling current is 10-100 pA. The motional current at the $n = 2$ resonant frequencies is typically 10 nA. Thus, for the high-coupling case, the resonances are obscured and modal parameters cannot be estimated.

It is clear from Fig. 4 that each input-output channel has a unique parasitic coupling characteristic so a feedforward filter which can "cancel" the coupling in a given channel will generally not perform well if implemented for other channels. Furthermore, it will be shown that the coupling is (slowly) time-varying, thus, the filter must be adaptive for achieving uniform suppression over the duration of an experiment. The relatively modest change in the coupling magnitude and phase as a function of frequency, however, suggests that a low-order filter can adequately model the parasitics over a broad frequency band. Thus, in the next sections we propose an adaptive filtering technique that can reduce the severity of the coupling by predicting its behavior in the frequency band containing the motional response based on a model that is identified from signals that lie out of this band. An advantage of the approach is that modification of the resonator or its electronics is not necessary since the cancellation is implemented in the signal processor that is used to gather input-

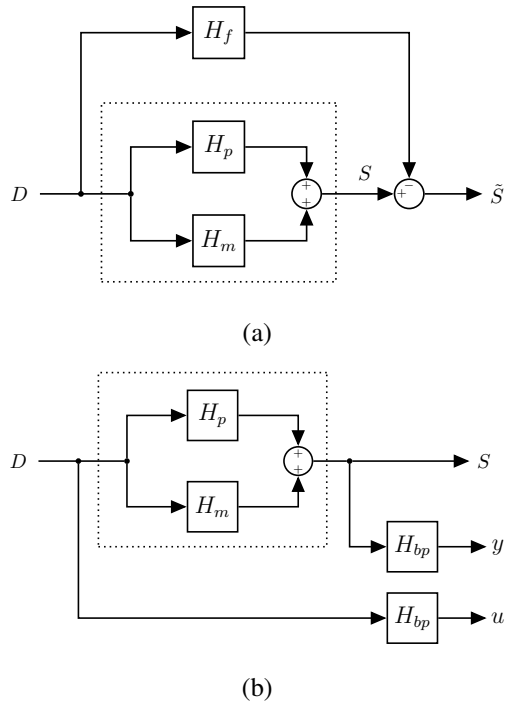


Fig. 5. (a) Block diagram for cancellation of the parasitic coupling using non-adaptive feedforward filter $H_f$. (b) Block diagram for identification of the parasitic coupling $H_p$.

output data from the resonator. Since the technique proposed in this paper is based on manipulating the input-output signals of the device, it is natural to ask if other techniques such as EAM could be applied to these resonators. The high gain of the trans-resistance buffers requires that they roll-off above 30 kHz in order to maintain stability. The resonator bias dither that is used in EAM would typically shift the sidebands associated with the motional response into the attenuating frequency band of the buffer where they would be subject to different magnitude and phase distortions so the subsequent demodulation using the carrier signal would produce a biased estimate of the motional frequency response. Thus, further development is required to adapt the EAM technique to these devices.

## III. Parasitic coupling identification

The approximate cancellation of the parasitic coupling requires the identification of a model. The system block diagram in Fig. 3(b) decomposes the measured frequency response into the sum of a motional component, $H_m$, and a parasitic coupling component, $H_p$. As shown in Fig. 4, there are circumstances in which the parasitic coupling dominates the frequency response measurement. Thus, it is desired to approximate $H_p$ over some frequency band so that a feedforward filter, denoted $H_f$ in Fig. 5(a), can be implemented to reduce its severity. In fact, the feedforward filter can be taken to be the identified parasitic model. In other words, when $H_f \approx H_p$ over some frequency band, then $\tilde{S}_1/D_1 \approx H_m$ in this band and, thus, the identification of the motional transfer function within the band is possible.

It is counterproductive to attempt to match $H_f$ to $H_p$ over the entire available bandwidth (DC to the anti-alias corner frequencies) because matching is only required in a neighborhood of the resonant modes. Without *a priori* knowledge of the modal frequencies, though, the cancellation should be achieved over a broad frequency band to capture die-to-die variability. For example, [9] shows that the nominal frequency of the $n = 2$ pair of modes can vary up to 500 Hz on the same wafer for this particular resonator design. A strategy must be devised so that the motional components in $S$ are not included in $H_f$, otherwise the feedforward filter will treat the motional components as part of the parasitic coupling. The approach used in this paper is to design the signal $u$ to have a double-pass band spectrum in which the stop-band encompasses the resonances whose properties are to be measured. Since $u$ is used as the "input" in the identification of $H_p$, the feedforward filter $H_f$ (which is the identified model of $H_p$) will not depend an any resonator dynamics in the stop-band. An example spectrum of $u$ is shown in Fig. 6 and is achieved by filtering broad-band white noise, i.e. $D$ is white, with band-pass filters $H_{bp}$ as shown in Fig. 5(b). The band-pass filters are implemented by the DSP that generates the test signals. Since all signals are multivariable, it is assumed that the band-pass filtering is applied to each variable in $S$, respectively $D$, to form $y$, respectively $u$. The parasitic coupling $H_p$ is estimated using $u$ and $y$, however, any resonator modes located in the pass-bands will be included as a part of the feedthrough model and are therefore subject to cancellation. The pass-bands can be designed to exclude the frequency bands where resonator modes are likely to exist and in this case the transfer function from $D$ to $y$, denoted $y/D$, is

$$y/D = H_{bp}\left(H_m + H_p\right) = \underbrace{H_{bp}H_m}_{\approx 0} + H_{bp}H_p.$$

The motional components are removed from $y/D$ because it is assumed they are located in the stop-band, which is approximately 10–15 kHz for the the spectrum shown in Fig. 6. Since $u/D = H_{bp}$, $H_p$ is identified subject to the weighting $H_{bp}$. Thus, it is expected that good matching of $H_p$ will be achieved in the pass-bands. The parasitic coupling, while frequency-dependent per Fig. 4, does not exhibit rapid gain and phase variations in the stop-band so it is posited that good matching will also be achieved across the (5 kHz) stop-band when good matching is achieved in the pass-bands. This is the foundation of the proposed parasitic cancellation technique: by identifying a parasitic model based on the pass-band signals, this model is expected to closely approximate $H_f$ in the stop band due to the relative simplicity of the coupling. The results in this paper support this conjecture.

Designing $u$ to identify $H_p$ does require some *a priori* knowledge of the device's resonant frequencies since it is assumed that the motional components of interest lie in the stop-band, however, considerable uncertainty in the exact location of the resonant modes is tolerated. Information on the resonator modal properties is generally available from, for example, finite element analysis so it is possible to design the stop-band without explicit knowledge of the modal frequencies in a particular device. Cancellation of the parasitic coupling is

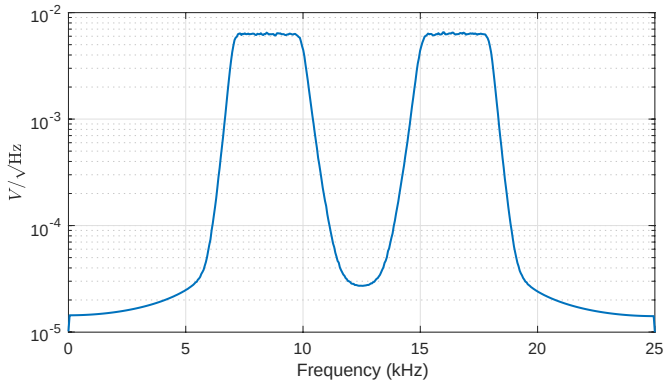


Fig. 6. Power spectrum of the input signal $u$ that is used to identify the parasitic coupling. The "stop band" from 10–15 kHz is the range in which suppression of the coupling is desired so that the motional response of the resonator can be measured.

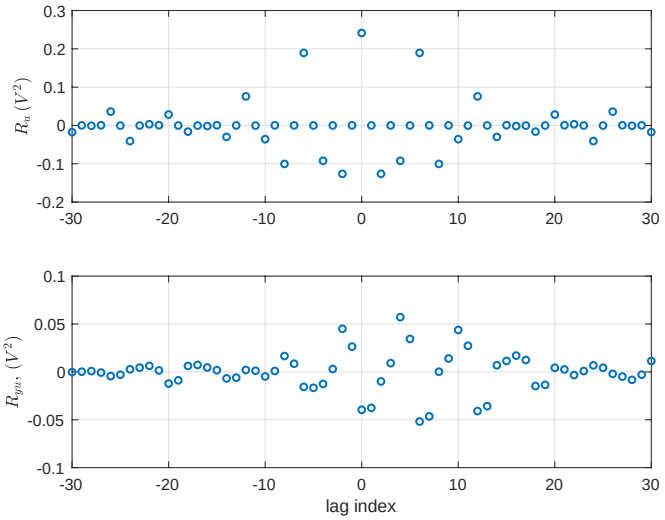


Fig. 7. Correlation functions $R_u$ and $R_{yu}$ corresponding to the $D_2$ input and the $S_2$ output for the "high coupling" resonator in Fig. 4.

achieved by setting $H_f$ to be the identified model of $H_p$ and implementing $H_f$ according to Fig. 5(a). Thus, the parasitic coupling is reduced in the frequency band containing the motional components, however, $H_f$ itself does not rely on this portion of the spectrum. The motional components are estimated using $D$ and $\tilde{S}$ in Fig. 5(a). The transfer function is

$$\tilde{S}/D = H_m + H_p - H_f$$

so if $|H_p - H_f| << |H_m|$ in the stop-band, then $H_m$ can be estimated using standard spectral estimation techniques applied to $D$ and $\tilde{S}$, eg. Welch's method, mentioned in Sec. II-B.

A finite impulse response (FIR) model of $H_p$ is identified because it can be simply extended to an adaptive implementation, however, the non-adaptive implementation is address first. A single input-output channel is considered for the sake of clarity, however, extension to the mutli-input/multi-output case is straightforward when all inputs are independent white sequences. Thus, for purposes of illustration, we consider input $D_2$ and output $S_2$ for the resonator with high coupling in Fig. 4. Since $D_2$ is white, $u$ is stationary and will possess an autocorrelation function $R_u$ like that shown in Fig. 7 (this is the autocorrelation of the signal whose spectrum is given in Fig. 6). If the device under test is time-invariant then $S_2$, and hence $y$, are also stationary and the cross-correlation function $R_{yu}$ can be determined from processing measurement sequences. An example of $R_{yu}$ is also shown in Fig. 7 and corresponds to the $S_2/D_2$ channel of the "high coupling" resonator in Fig. 4.

A causal FIR model of length $N$ is defined by the coefficients $\{h_f(0), h_f(1), \ldots, h_f(N-1)\}$, where $\{0, 1, \ldots, N-1\}$ are the lag indices. The FIR coefficient vector, denoted $\hat{h}_f$, is determined by solving the normal equations [13],

$$\hat{R}_{yu} = \hat{R}_u \hat{h}_f, \tag{2}$$

where $\hat{R}_u$ is the matrix of auto-correlation values of $R_u$, and $\hat{R}_{yu}$ is a vector of cross-correlation values of $R_{yu}$,

$$\begin{aligned}
\hat{R}_{yu} &= \begin{bmatrix} R_{yu}(0) & R_{yu}(1) & \cdots & R_{yu}(N-1) \end{bmatrix}^T \\
\hat{h}_f &= \begin{bmatrix} h_f(0) & h_f(1) & \cdots & h_f(N-1) \end{bmatrix}^T \\
\hat{R}_u &= \begin{bmatrix} R_u(0) & R_u(-1) & \cdots & R_u(-N+1) \\ R_u(1) & R_u(0) & \cdots & R_u(-N+2) \\ R_u(2) & R_u(1) & \cdots & R_u(-N+3) \\ \vdots & \vdots & \ddots & \vdots \\ R_u(N-1) & R_u(N-2) & \cdots & R_u(0) \end{bmatrix}
\end{aligned} \tag{3}$$

The superscript $(\cdot)^T$ denotes the transpose. Note that (2) assumes the coupling is exactly modeled by an FIR filter with length $N$. This is, of course, an approximation so we adopt a practical approach and assess the quality of fit for various filter lengths. Although $h_f$ is a model of the parasitic coupling, it is also used as the feedforward filter, hence the subscript $f$ is employed.

The cancellation performance of the FIR filter as a function of $N$ is determined by calculating $\hat{h}_f$ for various lengths and comparing the filter's frequency response to the empirical frequency response. For this comparison, the resonators are operated at atmospheric pressure so that the motional response is eliminated from the frequency response –the measurements in this case reveal the "pure" parasitic coupling. Off-line calculations of filters of different orders are computed from (2) and are shown in Fig. 8 using the $S_2/D_2$ channel from Fig. 4 for the comparison. The values of $R_u$, and hence $\hat{R}_u$ and its inverse, are computed analytically. Although $\hat{R}_u$ is positive definite, its condition number can be quite large for filter lengths greater than $N = 10$ so there is potential risk in amplifying uncertainty in $R_{yu}$ since the latter is estimated by averaging over a finite interval in both the off-line and adaptive implementations. Nevertheless, the frequency responses in Fig. 8 appear to show little difference for orders larger than $N = 9$. Differentiation between filters of higher orders is possible, though, by graphing $|H_p - H_f|$, where $H_p$ and $H_f$ represent the empirical frequency response and

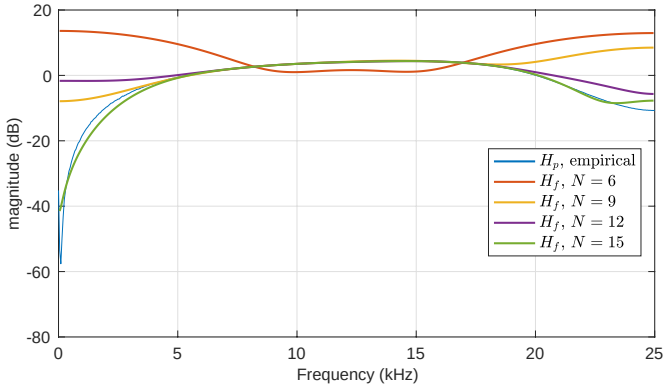


Fig. 8. Frequency responses of identified FIR filters of orders $N = \{6, 9, 12, 15\}$ compared to the $S_2/D_2$ channel empirical frequency response (the resonator is operated at atmospheric pressure so that only the parasitic coupling is present in the empirical frequency response).

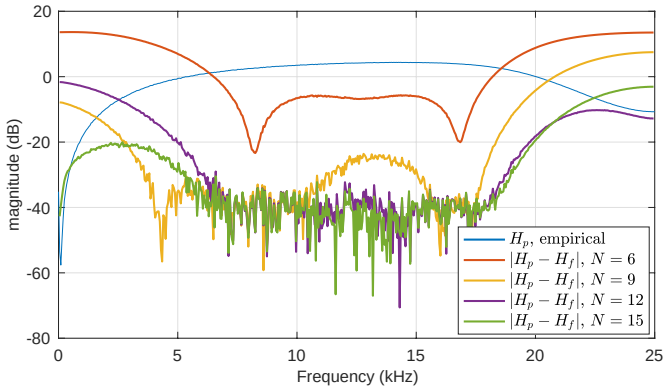


Fig. 9. Differences between the FIR filters' frequency responses and the empirical frequency response.

FIR filter frequency response, respectively. This is illustrated in Fig. 9 (there is some abuse of notation because Figs. 8 and 9 only show the $(2, 2)$ channels of $H_p$ and $H_f$). From this perspective, more uniform suppression in the 10-15 kHz stop band is achieved when $N \geq 12$, however, there is little difference between $N = 12$ and $N = 15$. Since the adaptive implementation requires the product of $\hat{R}_u^{-1}$ and $\hat{R}_{yu}$ there is an incentive to keep the filter order as low as practicable, thus, a filter order of $N = 12$ is selected for the adaptive filter discussed in the next section.

## IV. Adaptive Formulation

An adaptive implementation is appealing even when the coupling is time invariant because it combines identification and feedforward cancellation into a single framework that can simply be left running for the duration of an experiment. On the other hand, handling the device between tests may change the parasitic coupling especially if the device is disconnected from, and then reconnected to, the buffer board. In other words, although the parasitic coupling may considered to be time-invariant over the course of an experiment, it may not be invariant from one experiment to another especially if the die had been manipulated in the interim. In this case, a new identification test to determine the parasitics is required at the start of each experiment. The adaptive implementation gracefully accommodates such changes. Furthermore, it is also possible that the parasitic coupling is time-variant over the course of an experiment. This is the case for the devices tested for this paper and so the adaptive filter is necessary to continuously compensate for the coupling.

### A. Recursive estimation of $R_{yu}$

The feedforward filter can be converted into an adaptive implementation if $R_{yu}$ is recursively estimated with a forgetting factor. Since the input $u$ is stationary, $\hat{R}_u$ and $\hat{R}_u^{-1}$ are constant and are therefore computed off-line in the adaptive implementation (the FIR filter order now being fixed at $N = 12$ based on the analysis of Sec. III). When the parasitic coupling is time-variant, $S_2$ and $y$ are non-stationary and the feedfoward filter parameters need continuous updates. Thus, $R_{yu}$ is estimated over a horizon that is shorter than the time scale over which the parasitic coupling is expected to change. This is accomplished by updating $R_{yu}$ as new samples of $u$ and $y$ become available using the exponential weighting factor $\lambda$. The elements of the vector $v$ represent estimates of the first $N$ terms in the cross-correlation $R_{yu}$ function,

$$v(t+1) = \lambda v(t) + (1-\lambda)\,\bar{R}_{yu}(t), \tag{4}$$

where

$$\bar{R}_{yu}(t) = \begin{bmatrix} y(t)u(t) \\ y(t)u(t-1) \\ \vdots \\ y(t)u(t-N+1) \end{bmatrix}.$$

Note that $v$ is produced by low-pass filtering the products $y(t)u(t)$, $y(t)u(t-1)$, etc., with a unity DC gain discrete-time filter. The corner frequency of the filter is related to $\lambda$. Thus, the elements of $v$ are estimates of $R_{yu}(0)$, $R_{yu}(1)$, and so forth. The forgetting factor $\lambda$ determines the horizon over which $\hat{R}_{yu}$ is estimated. The first order difference equation (4) is exponentially stable when $|\lambda| < 1$ and the low-pass time constant $\tau_c$ is related to the forgetting factor by

$$\lambda = e^{-t_s/\tau_c} \tag{5}$$

where $t_s$ is the sample period. The FIR filter coefficients are updated according to

$$\hat{h}_f(t) = \hat{R}_u^{-1} v(t). \tag{6}$$

The block diagram in Fig. 10 shows the adaptive implementation where the "Corr" block computes $v$ and the product $\hat{R}_u^{-1} v$.

The single channel analysis of the preceding discussion is trivially extended to the multivariable case which involves identifying and implementing a two-input/two-output FIR filter to perform the parasitic coupling cancellation. Each channel is identified independently of the others in this multi-input case so $D_2$, respectively $D_1$, acts like a disturbance when determining the transfer functions associated with the $D_1$, respectively $D_2$, input channel. This produces larger variances in cross-correlation estimates for a given forgetting factor compared to the single-input case, however, since $D_1$ and

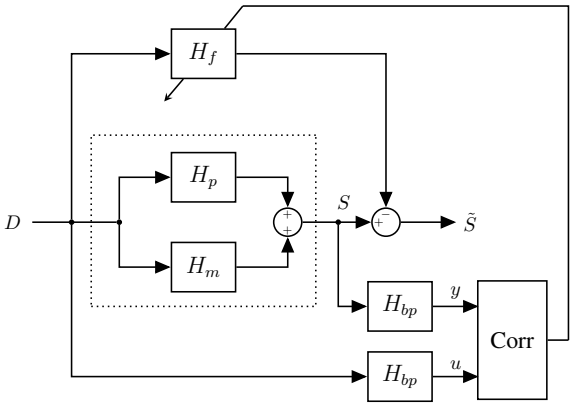


Fig. 10. Block diagram for adaptive implementation of the adaptive feedforward filter. The "Corr" block computes (4) and (6) in order to estimate the FIR coefficients.

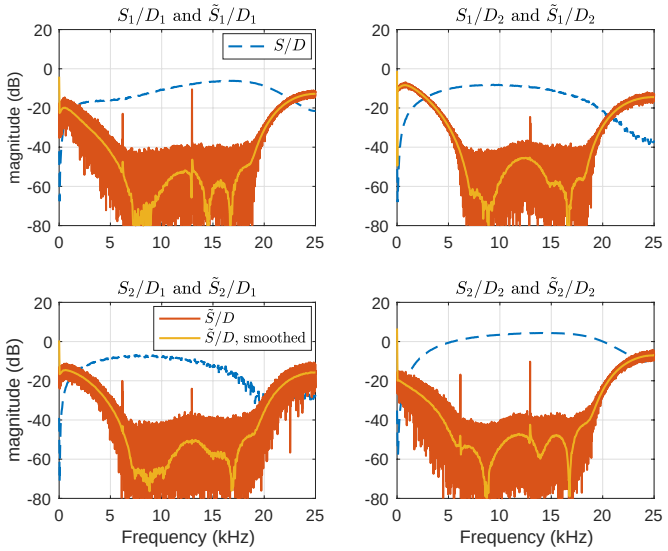


Fig. 11. The uncompensated empirical frequency response $S/D$ is compared to the compensated frequency response $\tilde{S}/D$. The compensated response reveals the $n = \{1, 2\}$ pairs of modes in the resonator. Further smoothing of the compensated estimate is used to assess the suppression of the parasitic coupling.

$D_2$ are independent, the smoothing filter time constant $\tau_c$ can be adjusted such that the "disturbances" are effectively eliminated. For the devices under test the time constant is selected to be $\tau_c = 10$ seconds. This choice represents a balance between low-variance estimates of $R_{yu}$ and the drift in the parasitic coupling.

### *B. Adaptive cancellation results*

Typical cancellation performance of the adaptive filter is shown in Fig. 11 where the original parasitic coupling is included for comparison (denoted "$S/D$" in this figure). The motional components are identified from spectral estimates of signals $D$ and $\tilde{S}$. A frequency resolution (0.1 Hz) is necessary to resolve the resonator modes. It appears that at least 30dB of reduction is achieved in the 10-15 kHz stop band and, consequently, the resonator's $n = 2$ modes are clearly revealed (the "$\tilde{S}/D$" traces in Fig. 11). Details in a neighborhood of these modes are shown in Fig. 12. These non-parametric frequency response estimates are clean enough to obtain accurate measurements of modal frequencies and quality factors. The frequency response phase is also estimated but is not shown due to space constraints. Further frequency domain smoothing of the compensated frequency response yields more quantitative information on the degree of coupling suppression (denoted "$\tilde{S}/D$, smoothed" in Fig. 11). Note that in the pass-bands associated with the signal $u$ (7-10 kHz, and 15-18 kHz), the parasitic coupling suppression appears to be greater than the suppression in the stop-band (10-15 kHz). This is not surprising because the coupling is only estimated using the components of $S$ that lie in the pass-bands, thus, the matching is best in those bands.

Although the spectrum of $u$ was designed to identify and suppress the parasitic coupling in the stop-band, the parasitic coupling is also matched to some extent for frequencies below the lowest passband corner frequency (7 kHz). The adaptive filter also compensates the parasitics in this lower frequency region and reveals the $n = 1$ pair of modes at approximately 6.2 kHz. The $n = 1$ modes are the lowest frequency resonant modes in this resonator. Both of the $n = 1$ modes appear to be missing from the $S_1/D_2$ channel. This is a consequence of how the mode shapes couple to the electrode layout in Fig. 1. Since the physical electrode arrangement is optimized for the $n = 2$ pair, specifically, for exciting and sensing the $2\theta$ dependence of the mode shapes associated with the $n = 2$ modes, it is possible that modes other than the $n = 2$ pair may not be sufficiently excited or sensed because their mode shapes are different from the $n = 2$ pair. In fact, this is what occurs for the $n = 1$ modes whose mode shapes have a $1\theta$ dependence. Closer inspection of the multi-channel frequency responses in a neighborhood of the $n = 1$ modes reveals that that $D_2$ weakly excites the higher frequency $n = 1$ mode and that the lower frequency mode is not detectable from $S_1$. Thus, both $n = 1$ modes are absent from channel $S_1/D_2$.

### *C. Time-varying characteristic of the parasitic coupling*

This section provides experimental evidence that the parasitic coupling is time-variant so a fixed feedforward filter will not necessarily perform well at all times in terms of cancelling the coupling. Thus, if a fixed filter is implemented, it must be periodically updated to reflect the current state of coupling. Updating the feedforward filter, though, is what the adaptive implementation accomplishes in an autonomous manner. Identifying the cause(s) of the time-variance of the parasitic coupling has remained elusive for these devices. The inadequacy of a time-invariant feedforward filter is demonstrated by conducting the following experiment: the filter is allowed to adapt at the beginning of an experiment at which point an estimate of $\tilde{S}/D$ is made to assess the coupling suppression; next, the filter coefficients are frozen for two hours after which another measurement of $\tilde{S}/D$ is performed; finally, the filter is allowed to adapt and another measurement of $\tilde{S}/D$ is performed. The resonator is operated at atmosphere pressure in these experiments to emphasize the parasitic

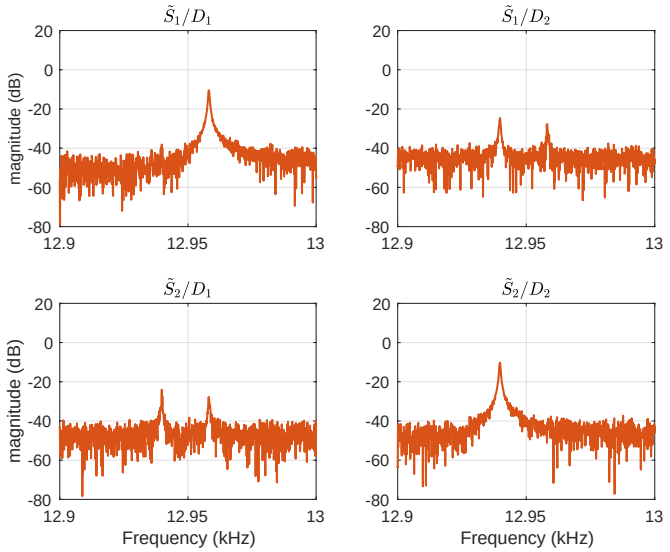


Fig. 12. Frequency response estimate from Fig. 11 in a neighborhood of the $n = 2$ modes.

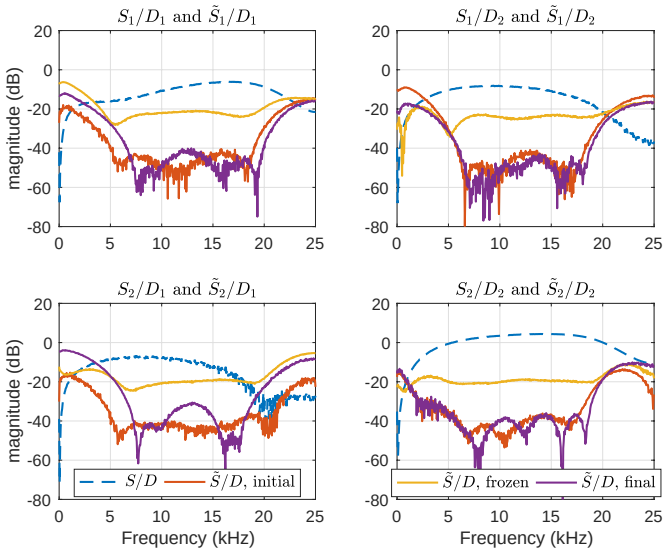


Fig. 13. Parasitic coupling suppression using adaptive versus fixed-coefficient feedforward filters. The resonator is at atmospheric pressure to eliminate the motional response and emphasize the parasitic coupling.

coupling. The results of this experiment are summarized in Fig. 13. The frequency responses labeled "$\tilde{S}/D$, initial" are those measured after the first adaptation. The "$\tilde{S}/D$, frozen" frequency responses are the measurements made after two hours using the coefficients from the initial adaptation period. It is clear that this filter, which successfully suppressed the parasitic coupling at the start of the experiment, no longer provides the same level of cancellation at later times. When the filter is allowed to adapt again to the present state of coupling, however, good cancellation performance is recovered ("$\tilde{S}/D$, final" frequency responses in Fig. 13). The filter coefficients corresponding to the "Initial" and "Final" filters are shown in Fig. 14 and demonstrate that the filter is indeed changing and that relatively small changes in the coefficient values can have a significant impact on the level of suppression. This is not surprising, however, because good cancellation requires very close matching of the magnitude and phase of the parasitic coupling by the filter, i.e. achieving 40 dB of suppression corresponds to a deviation of less than one percent from the actual parasitic coupling.

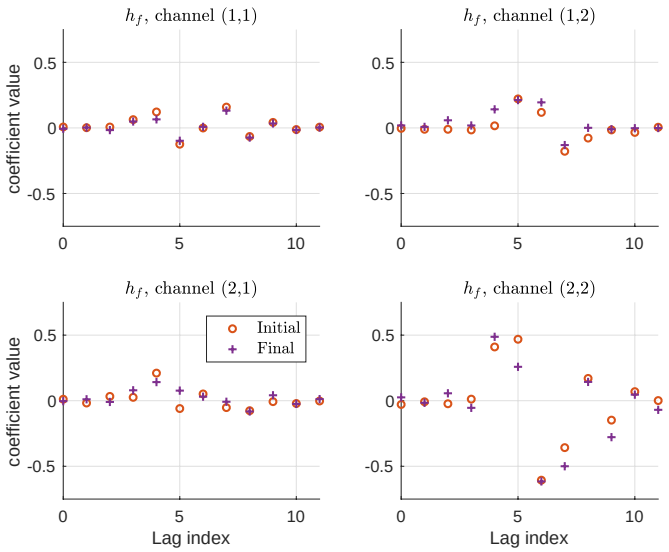


Fig. 14. Coefficients of feedforward filter at the beginning ("Initial") and end ("Final") of a two hour experiment.

### *D. Cancellation performance on devices with low coupling*

The appeal of the proposed adaptive cancellation method will be considerably strengthened if it can be demonstrated to leave the empirical frequency response estimates intact in devices with low parasitic coupling. This is demonstrated in this section by testing a resonator possessing low parasitic coupling. The resonator is identical in design and electrode configuration as the schematic in Fig. 1, however, the base wafer resistivity is much larger than that of the devices exhibiting high coupling (cf. Sec. II-B). Nevertheless, implementing the feedforward compensation is still performed and the desired outcome is achieved: the feedforward filter manages to further reduce the coupling in the stop band yet does not modify the frequency response in a neighborhood of the modes. The input spectra remain the same as the previous experiments, i.e. Fig. 6. The uncompensated and compensated transfer function estimates are shown in Fig. 15 with detail of the $n = 2$ modes in Fig. 16. Note that the $n = 2$ modal frequencies are about 600 Hz higher that the previous device but since they still lie within the stop-band, their frequency response functions are not modified by the feedforward filter. Thus, the cancellation method can be applied to a resonator without *a priori* information on the level of coupling or modal frequency values. It is interesting to note that the feedforward filter *increases* the coupling outside of the pass-band and stop-band regions because the FIR filter estimation technique essentially ignores anything outside of the pass-bands.

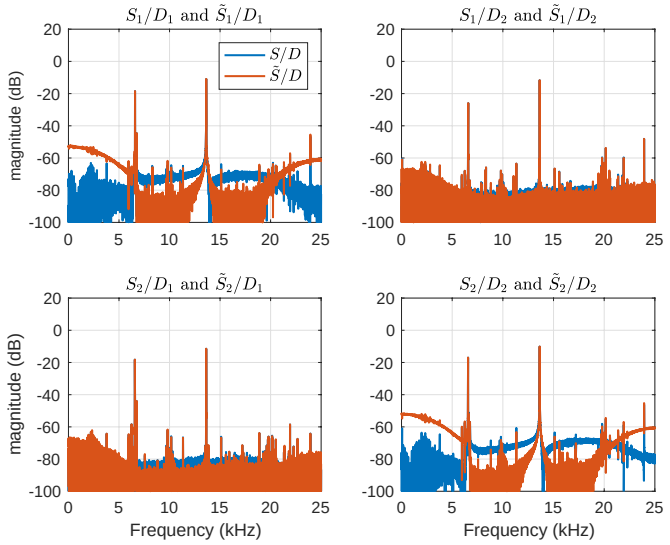


Fig. 15. Resonator with low parasitic coupling. The feedforward filter still reduces the coupling in the stop-band region.

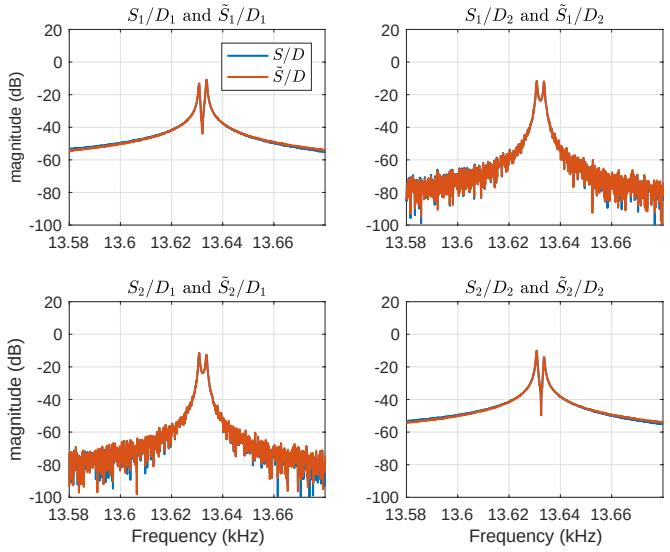


Fig. 16. Detail of resonator with low parasitic coupling in a neighborhood of the $n = 2$ pair of modes. The feedforward filter does not modify the frequency response.

## V. Conclusion

This paper has demonstrated an adaptive feedforward filter that cancels the parasitic coupling in a user-specified frequency band in a MEMS resonator. The compensated measurement can then be processed to estimate the frequency response of the motional components inside this band. For the resonators tested in paper, the band was broad enough to contain the $n = 2$ pair of modes for all conceivable devices of that particular design, i.e. resonator-to-resonator variability is gracefully handled. The success of the method does rely on the relative simplicity of parasitic coupling since a low-order FIR coupling model is anticipated to interpolate the parasitic coupling in the stop-band associated with the double band-pass filtered input as the pass-bands are the frequency intervals over which the parasitic coupling is actually identified. Cancellation of 30 dB of parasitic coupling is typical across the entire stop-band and even 40 dB is achieved in some cases. Despite the simplicity of the coupling, gain variations of 3-4 dB occur in the stop-band making compensation techniques based on estimating the coupling at a single frequency unlikely to perform well across the entire stop-band. The proposed method is implemented in the downstream signal processing so no design changes are imposed upon the resonator or its test electronics. The method is also able to identify multi-input/multi-output devices by simultaneously using all inputs. Although it may be difficult to integrate this technique as a part of normal device function, it can certainly be used to accelerate resonator development because effort need not be devoted toward developing on-chip compensation techniques in order to make basic modal parameter measurements. Based on practical test results, though, the technique cannot reveal motional components that lie 40 dB below the parasitic coupling level, at least for the resonator under study.

The adaptive implementation is able continuously update the feedforward filter so that any changes in the parasitic coupling are still cancelled by 30-40 dB, however, even if the coupling is time-invariant, the adaptive implementation combines the identification and feedforward cancellation features into one framework. This makes the approach essentially "turn-key" once a suitable spectrum for $u$ and the FIR filter order have been determined for a given class of resonators. The electrode arrangement and test signal details were tailored to the $n = 2$ modes, however, other modes can be identified by redesigning the band-pass filters and possibly the electrode assignment The tested resonators are low-frequency devices, however, it may be possible to extend this technique to the identification of modes in the RF range by demodulating $u$ and $y$ in Fig. 5 –a DSP can still be employed for filtering the resulting baseband signals. This promising direction will be addressed in future publications.

## Acknowledgement

The authors thank the staff of the UCLA Nanoelectronics Research Facility. This research did not receive any specific grant from funding agencies in the public, commercial, or not-for-profit sectors.

## References

[1] J. Lee and A. Seshia, "Parasitic feedthrough cancellation techniques for enhanced electrical characterization of electrostatic microresonators," *Sensors and Actuators A: Physical*, vol. 156, no. 1, pp. 36 – 42, 2009.

[2] J. Giner, A. Uranga, E. Marig, J. L. Muoz-Gamarra, E. Colinet, N. Barniol, and J. Arcamone, "Cancellation of the parasitic feedthrough current in an integrated CMOS-MEMS clamped-clamped beam resonator," *Microelectronic Engineering*, vol. 98, no. Supplement C, pp. 599 – 602, 2012.

[3] J. Arcamone, E. Colinet, A. Niel, and E. Ollier, "Efficient capacitive transduction of high-frequency micromechanical resonators by intrinsic cancellation of parasitic feedthrough capacitances," *Applied Physics Letters*, vol. 97, no. 4, p. 043505, 2010.

[4] A. Uranga, J. Verd, J. L. Lopez, J. Teva, F. Torres, J. J. Giner, G. Murillo, G. Abadal, and N. Barniol, "Electrically enhanced readout system for a high-frequency CMOS-MEMS resonator," *ETRI Journal*, vol. 31, no. 4, pp. 478–480, 2009.

[5] A. T. H. Lin, J. E. Y. Lee, J. Yan, and A. A. Seshia, "Enhanced transduction methods for electrostatically driven MEMS resonators," in *2009 International Solid-State Sensors, Actuators and Microsystems Conference (TRANSDUCERS)*, June 2009, pp. 561–564.

[6] C. T.-C. Nguyen, "Micromechanical Signal Processors," Ph.D. dissertation, University of California, Berkeley, 1994.

[7] K. V. Shcheglov and A. D. Challoner, "Isolated planar gyroscope with internal radial sensing and actuation," US Patent US7 040 163B2, May 9, 2006.

[8] D. Schwartz, D. Kim, P. Stupar, J. DeNatale, and R. M'Closkey, "Modal parameter tuning of an axisymmetric resonator via mass perturbation," *J. Microelectromech. Syst.*, vol. 24, no. 3, pp. 545–555, June 2015.

[9] A. H. Behbahani, D. Kim, P. Stupar, J. DeNatale, and R. T. M'Closkey, "Tailored etch profiles for wafer-level frequency tuning of axisymmetric resonators," *J. Microelectromech. Syst.*, vol. 26, no. 2, pp. 333–343, April 2017.

[10] Y.-C. Chen, R. T. M'Closkey, T. A. Tran, and B. Blaes, "A control and signal processing integrated circuit for the jpl-boeing micromachined gyroscopes," *IEEE Transactions on Control Systems Technology*, vol. 13, no. 2, pp. 286–300, March 2005.

[11] H. Ge and R. MCloskey, "Simultaneous angular rate estimates extracted from a single axisymmetric resonator," *IEEE Sensors Journal*, vol. 17, no. 22, pp. 7460–7469, Nov 2017.

[12] P. Welch, "The use of Fast Fourier Transform for the estimation of power spectra: A method based on time averaging over short, modified periodograms," *IEEE Trans. Audio Electroacoust.*, vol. 15, no. 2, pp. 70–73, 1967.

[13] B. Buttkus, *Spectral Analysis and Filter Theory in Applied Geophysics*. Springer-Verlag, 2000.